# Prediction Method for Cavitation Erosion Based on Measurement of Bubble Collapse Impact Loads

# Prediction Method for Cavitation Erosion Based on Measurement of Bubble Collapse Impact Loads

**S Hattori [1], T Hirose [1], K Sugiyama [2]**

[1] Graduate School of Engineering, University of Fukui, 3-9-1 Bunkyo, Fukui-shi, Fukui 910-8507, JAPAN
[2] Ebara Research Co., Ltd., 4-2-1 Honfujisawa, Fujisawa-shi, Kanagawa 251-8502, JAPAN

hattori@mech.fukui-u.ac.jp

**Abstract**. The prediction of cavitation erosion rates is important in order to evaluate the exact life of components. The measurement of impact loads in bubble collapses helps to predict the life under cavitation erosion. In this study, we carried out erosion tests and the measurements of impact loads in bubble collapses with a vibratory apparatus. We evaluated the incubation period based on a cumulative damage rule by measuring the impact loads of cavitation acting on the specimen surface and by using the "constant impact load - number of impact loads curve" similar to the modified Miner's rule which is employed for fatigue life prediction. We found that the parameter $\sum(F_i^{\alpha} \times n_i)$ ($F_i$: impact load, $n_i$: number of impacts and $\alpha$: constant) is suitable for the evaluation of the erosion life. Moreover, we propose a new method that can predict the incubation period under various cavitation conditions.

## 1. INTRODUCTION

Cavitation often occurs in the contact area between solids and liquids, in fluid machineries, pipes, ship propellers, valves and so on. The erosion is a phenomenon that erodes the component surface sponge-like. Cavitation erosion is a serious problem that brings a performance reduction of an apparatus or a life reduction by component failure. The measurement of impact loads in bubble collapses (bubble collapse impact loads) helps us to predict the cavitation erosion.

Hattori et al. (1998) measured bubble collapse impact loads using a venturi test facility and a vibratory apparatus, and clarified the relation between the cumulative impact energy $\sum F_i^2$ ($F_i$: impact load) obtained from the impact load distribution and the erosion volume loss rate. For low $\sum F_i^2$ (near the cavitation damage threshold), however, the relation between $\sum F_i^2$ and the volume loss has not yet been clarified. On the other hand, Iwai et al. (1988) reported a good proportional relation of the incubation period or the volume loss rate in the steady period in a vibratory apparatus with the fatigue damage $\sum(n_i/N_i)$ calculated at stress amplitudes more than a certain threshold value. However, there is an issue that a basic S-N curve against the erosion rate has to be assumed and the threshold value of the impact loads without the influence of erosion has to be found experimentally. Soyama et al. (2007) carried out a cavitation test using a sheet of pure aluminum glued to a pump impeller, and obtained the bubble collapse impact loads from the deformation of the aluminum sheet. They proposed a threshold for the erosion energy so that erosion does not occur. However, the physical meaning of the erosion energy threshold was not clarified.

In this study, we carried out erosion tests and measured the bubble collapse impact loads under

various cavitation conditions. We discuss a prediction method for the incubation period of the cavitation erosion.

## 2. MATERIALS AND TEST METHOD

### 2.1 Materials

The test materials are pure aluminum of A1050 and A1070BD-F as accelerated test material, S55C carbon steel for machine structural use and S15C low carbon steel, and SUS304 austenite stainless steel with high corrosion resistance. The chemical compositions and the physical and mechanical properties of these materials are listed Tables 1 and 2, respectively. Erosion test results (except for A1070BD-F) are taken from the date base constructed in our laboratory (Hattori et al., 2004). The size of each test specimen is 25 mm in diameter and 5 mm in thickness. The test specimen surface was mirror-finished by buffing after being polished with emery paper up to grade #1200.

Table 1  Chemical compositions of test materials (mass%)

| Material | Si | Fe | Cu | Mn | Mg | Zn | V | Ti | Al |
|----------|-----|-----|------|------|------|------|------|------|-------|
| A1050 | 0.09 | 0.14 | 0.01 | 0.01 | 0.01 | 0.01 | 0 | 0.01 | 99.5 |
| A1070BD-F | 0.07 | 0.14 | 0 | 0 | 0.01 | 0 | 0.01 | 0.01 | 99.75 |
|  | C | Si | Mn | P | S | Cr | Ni | | |
| S15C | 0.15 | 0.25 | 0.47 | 0.015 | 0.015 | - | - | | |
| S55C | 0.54 | 0.27 | 0.82 | 0.016 | 0.017 | - | - | | |
| SUS304 | 0.071 | 0.48 | 1.21 | 0.025 | 0.022 | 18.47 | 8.21 | | |

Table 2  Physical and mechanical properties of test materials

| Material | $\rho$ g/cm$^3$ | E GPa | $\sigma_B$ MPa | HV |
|----------|------|------|------|------|
| A1050 | 2.71 | 71 | 178 | 33 |
| A1070BD-F | 2.67 | 71 | 106 | 41 |
| S15C | 7.87 | 206 | 388 | 151 |
| S55C | 7.87 | 204 | 701 | 238 |
| SUS304 | 7.98 | 200 | 618 | 209 |

### 2.2 Test Method

The cavitation erosion tests were carried out in a stationary specimen method by using a vibratory apparatus as specified in the ASTM standard G32-03 (ASTM Designation, G32-03, 2005). A vibrating disk of 16 mm in diameter made of erosion resistant SUS304 steel was screwed into the amplifying horn of an oscillator, and the test specimen was placed in close proximity to the vibrating disk as shown in Fig. 1. To produce various cavitation conditions, the distance between the vibrating disk and the test specimen (standoff distance) was adjusted to be 1, 2 and 4 mm. The resonance frequency of oscillator was 19.5 kHz, and the double (peak to peak) amplitude of the vibrating disk was 50 μm. After using the vibrating disk for 10 hours, the disk was replaced by a new one. The test liquid was deionized water, and kept at 25±2 degrees C with a temperature control device. The test specimen was removed periodically after predetermined time intervals, and weighed with a precision balance
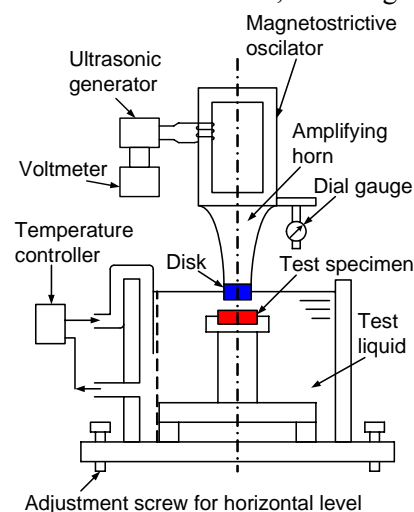


Fig. 1  Vibratory apparatus

(sensitivity of 0.01 mg) after cleaning with acetone in an ultrasonic bath. The test result was expressed by using the MDE (Mean Depth of Erosion), i.e. the mass loss divided by the density of material and the eroded area.

The bubble collapse impact loads were measured under the same conditions as in the cavitation erosion test by using a piezo ceramic transducer (sensor) instead of the test specimen. The bubble collapse impact loads were measured for 1 minute. Fig. 2 shows an illustration of the sensor structure. The piezo ceramic for detecting impact loads is a disk of 5 mm in diameter and 0.2 mm in thickness. The piezo ceramic was sandwiched between the 3 mm detection rod made of Ti and the reflection rod of Cu, and fixed with a conductive adhesive. An epoxy resin agent was used to fill in the space between the part of the pressure detector and the acrylic resin pipe for making it vibration-proof, water-proof and for protection from breakage of the ceramic disk. The sensor performance depends on the surface profiles of the detection rod and the reflection rod and on the adhesive condition of the piezo ceramic. To eliminate the differences in sensor performance, we carried out a steel ball drop test to obtain a calibration coefficient for the sensor before the measurement of bubble collapse impact loads. In the steel ball drop test, a steel ball (0.134g) made of SUS304 was dropped on the detection surface of the sensor, and the output waveform in Fig. 3 was read using an oscilloscope. The maximum voltage $\Delta V[V]$ and the hold time of the impact load $\Delta T[\mu s]$ were obtained. The appropriate calibration coefficient of the sensor was obtained from the relation between the voltage and the impact load. The relation between the voltage V and the impact load F of the sensor used in this study was *F=1.83V* as shown in Fig. 4.

Fig. 5 shows the diagram for the measurement of the bubble collapse impact loads. The output signal obtained from the sensor was passed through the highpass filter to cut the low frequencies, and then fed into the computer with A/D conversion after being processed in the peak-hold circuit. To consider the influence of the voltage reduction in the circuit, we determined the calibration coefficient of the circuit from the relation between the input voltage and the output voltage of a the pulse wave (frequency is 1 kHz and height of pulse wave is adjusted to be 0 to 2.5 V). The pulse wave was generated using a function generator and the output voltage was obtained from the mode value of the height of the pulse wave after it passed through the circuit. The relation between the input voltage $V_{in}$
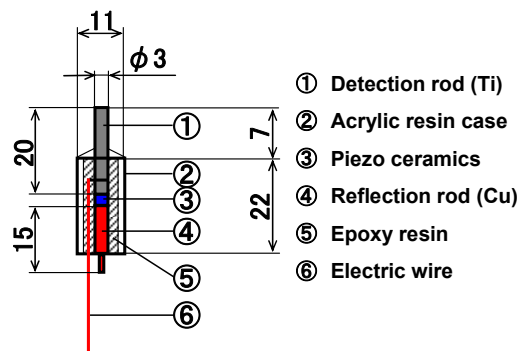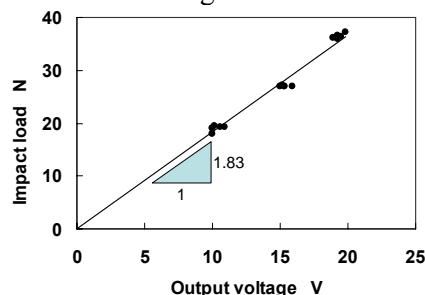


Fig. 2  Sensor



Fig. 3  Output waveform obtained
from steel ball drop test



Fig. 4  Relation between
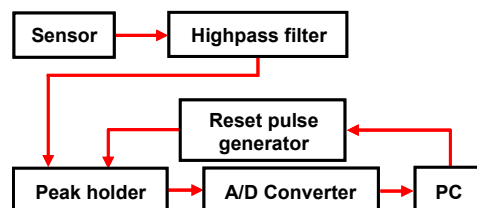output voltage and impact load



Fig. 5  Diagram for measurement of
bubble collapse impact loads

and the output voltage $V_{out}$ of the measuring system used in this study was $V_{in}=3.33V_{out}$. Therefore, we were able to obtain bubble collapse impact loads and their counts using the calibration factor of the sensor and the circuit.

## 3. TEST RESULTS AND PROPOSAL OF PREDICTION EQUATION

### 3.1 Test Result of Cavitation Erosion

Fig. 6 shows the MDE curves at standoff distances of 1, 2 and 4 mm between the vibrating disk and the specimen for pure aluminum A1050 and A1070BD-F. Fig. 7 shows the curves for the ferrous steels SUS304, S15C and S55C. Every MDE curve passes through an incubation period with low erosion rate and then increases linearly to reach a maximum rate period for each material. When each material is compared with the same exposure time, the MDE is high for the soft material A1050 and it is low for the hard material SUS304. This corresponds to our previous finding that the erosion rate has a good correlation with the hardness (Hattori et al., 2004).

Table 3 shows the incubation period for each material. The periods were obtained from Figs. 6 and 7 as the point of intersection of the extended straight line of the slope of the maximum rate period with the axis of the exposure time. The incubation period of A1050 with low hardness is short and that of S55C with high hardness is long. This is because cracks initiate easily for low hardness materials, because plastic deformation can occur even at low impact loads, when the various impact loads act on the material surface.
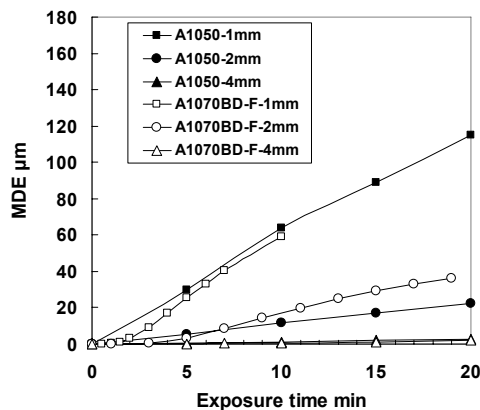

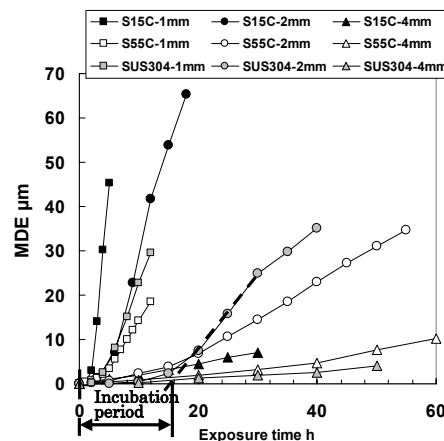
Fig. 6  MDE curves for A1050 and A1070BD-F



Fig. 7  MDE curves for S15C, S55C and SUS304

Table 3  Incubation period of test materials

| Material | Incubation period [min] | | |
| --- | --- | --- | --- |
| | Stand off distance | | |
| | 1mm | 2mm | 4mm |
| A1050 | 0.7 | 1.3 | 2.4 |
| A1070BD-F | 2.2 | 3.8 | 7.5 |
| S15C | 128 | 324 | 600 |
| S55C | 198 | 660 | 1410 |
| SUS304 | 240 | 840 | 1320 |

### 3.2 Measurement of Bubble Collapse Impact Loads

Fig. 8 shows the result of the bubble collapse impact loads measured with the sensor which was located at standoff distances of 1, 2 and 4 mm. Several thousand counts were detected for small impact loads and several counts with large impact loads. The distributions at the various distances are very similar, and the frequency of the large impact loads is higher at lower standoff distances.
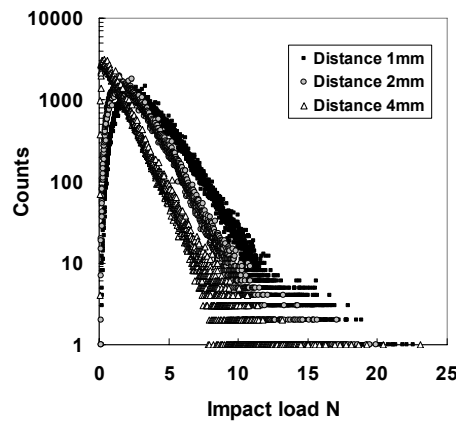
Fig. 8  Distribution of bubble collapse impact loads

### 3.3 Method for Prediction of Incubation Period

When the impact load $F_i$ acts on the specimen surface during the holding time $\Delta T$, the impact energy e is given (De and Hammitt, 1982; Hattori et al., 1985) by

$$e = \Delta T / \rho c \times F_i^{\,2} \qquad (1)$$

where $\rho$ is the density of the test liquid and c is the sound velocity in the liquid. If the holding time $\Delta T$ is assumed to be constant irrespective of the magnitude of the impact load acting on the specimen, the cumulative impact energy E for various impact loads $F_i$ on the specimen surface can be assumed to obey

$$E \propto \sum F_i^{\,2} \qquad (2)$$

That means the cumulative impact energy E is in proportion to the cumulative square value of impact loads ($\sum F_i^2$). $\sum F_i^2$ can be calculated with $\sum (F_i^2 \times n_i)$ using the impact load $F_i$ and its counts $n_i$ obtained from the measurement of the bubble collapse impact loads.

Fig. 9 shows the relation between $\sum F_i^2$ and the maximum erosion rate $MDER_{max}$ at various standoff distances obtained in this study. $MDER_{max}$ is the maximum slope in the maximum rate period of the MDE curve. $MDER_{max}$ increases linearly with $\sum F_i^2$ for all materials. The linear relation between
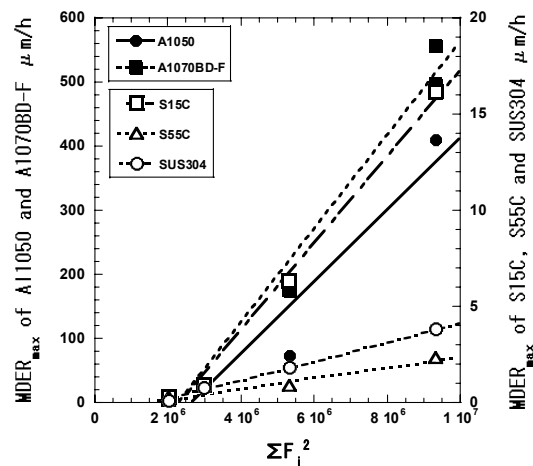


Fig. 9  Relation between $\sum F_i^2$ and $MDER_{max}$

$\sum F_i^2$ and the erosion rate was reported (Hattori et al., 1998), but regarding the result obtained in this study, the erosion rate becomes extremely low at values $\sum F_i^2$ of $1\sim2\times10^6$ and the existence of a threshold value for $\sum F_i^2$ without erosion is observed. To obtain a clear threshold value, however, further long-term tests at low cavitation intensities are required. Therefore, we discuss the prediction method from another viewpoint.

Hammitt et al. (1980) reported that the erosion proceeds by fatigue failure. Vaidya and Preece et al. (1978) reported that striation was observed on the eroded surface of Al-4%Cu alloy. The damage mechanism of components subjected to cavitation bubble collapse impact loads is therefore regarded as fatigue failure under the variable amplitude stress. We thus discussed the cavitation erosion from the viewpoint of fatigue life.

The linear cumulative damage rule is one of the prediction methods for the fatigue life under variable amplitude loading. Fig. 10 shows a schematic S-N curve on a double logarithmic scale. The slope part is given by

$$\sigma_i^\alpha \times N_i = C \tag{3}$$

Nakamura et al. (1981) proposed that the S-N curve on a double logarithmic scale should be used to predict the fatigue life. The fatigue damage is given by the cycle ratio $n_i/N_i$ when $\sigma_i$ is repeated $n_i$ times under variable amplitude stress. It is assumed that the damage at each stress level is independent and is accumulated linearly. It is further assumed that the material ruptures when the sum of the cycle ratios $n_i/N_i$ reaches unity. This sum is given by

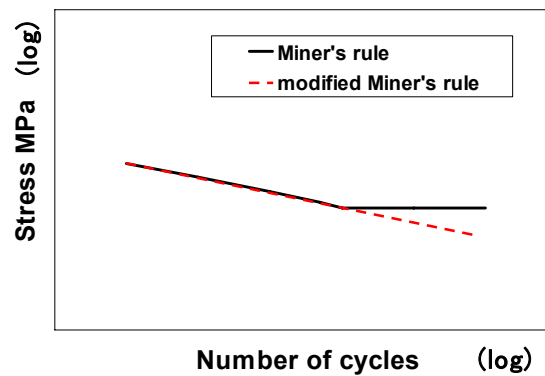$$D = \sum n_i/N_i = 1 \tag{4}$$



Fig. 10   S-N curves

The solid line in Fig. 10 shows the S-N curve in order to predict the fatigue life using Miner's rule, assuming that fatigue damage does not occur below the fatigue limit. The broken line in Fig. 10 is based on the modified Miner's rule which assumes that all stresses contribute equally to the fatigue damage. The result was that fatigue damage is accumulated due to the stress even below the fatigue limit under variable amplitude stress, when the stress is combined with stresses above the fatigue limit (de Jonge and Nederveen, 1980). The modified Miner's rule is nowadays generally used (de Jonge and Nederveen, 1980) to evaluate fatigue damage.

Since many impact loads at various intensities are measured in cavitation bubble collapses, the modified Miner's rule under the variable amplitude loading is applied to the prediction of cavitation erosion. The incubation period is defined as the point of intersection of the extended straight line of slope of the maximum rate period with the axis of exposure time (ASTM Designation, G32-03, 2005), and the termination of incubation period is well assumed to coincide with macroscopic fatigue failure. The incubation period has been discussed based on the accumulation of fatigue damage.

The prediction method of cavitation erosion was constructed on the basis of the modified Miner's rule by using the relation between the impact load $F_i$ and the number of cycles per unit time $n_i$ obtained from the measurement of bubble collapse impact loads at the various standoff distances. The incubation periods were obtained from the erosion test at the various standoff distances. Since it is impossible to measure the impacted area, we cannot convert the force to a stress. Therefore, the F-N curve was used. N is the impact number at the termination of the incubation period with constant impact load F. Since a test with a constant impact load $F_i$ cannot be carried out for cavitation erosion, the impact number at the termination of incubation period $N_i$ is basically unknown. But, the F-N curve is derived using constant parameters of $\alpha$ and C in

$$F_i^{\alpha} \times N_i = C \tag{5}$$

The parameter $\sum n_i/N_i$ is the cumulative damage per unit time. The incubation period $t_d$ (the subscript d indicates the standoff distance) finishes when $\sum n_i/N_i$ becomes unity. $t_d$ is therefore given as

$$t_d = \frac{1}{\sum n_i/N_i} \tag{6}$$

To determine the constants $\alpha$ and C, the unknown number $N_i$ in Eq. (5) is expressed by $F_i$ and the constants $\alpha$ and C, and then substituted into Eq. (6). The following equation results.

$$\frac{1}{C} \sum \left( F_i^{\alpha} \times n_i \right) = \frac{1}{t_d} \tag{7}$$

For a given material, the constants $\alpha$ and C are independent of the impact load $F_i$, the number of cycles $n_i$ and the incubation period $t_d$ at standoff distances of 1 and 2 mm. Therefore Eq. (7) with the data at the standoff distance of 1 mm was divided by Eq. (7) with the data at the standoff distance of 2 mm, which gives the following relation.

$$\frac{\sum F_{i,1}^{\alpha} \times n_{i,1}}{\sum F_{i,2}^{\alpha} \times n_{i,2}} = \frac{t_2}{t_1} \tag{8}$$

Since $t_d$, $F_i$ and $n_i$ are already given, the constant $\alpha$ can now be determined with a trial & error method using Eq. (8). After $\alpha$ is determined, the constant C can be obtained from Eq. (7). Since the constants $\alpha$ and C are different depending on the material, it is necessary to find them for each material. Table 4 shows the values of $\alpha$ and C for the various materials.

Table 4  $\alpha$ and C of each material

| Material | $\alpha$ | C |
|---|---|---|
| A1050 | 2.6 | 4.5E+05 |
| A1070BD-F | 2.0 | 5.3E+05 |
| S15C | 3.7 | 2.0E+05 |
| S55C | 5.1 | 6.1E+06 |
| SUS304 | 5.4 | 1.4E+07 |

**3.4 Predicted Results for Incubation Period**

The parameter $\sum F_i^2$ has been used previously to evaluate the erosion (Hattori et al., 1998). We have already discussed the erosion using the parameter $\sum (F_i^{\alpha} \times n_i)$ in Eq. (7). Fig. 11 shows the relation between the parameter $\sum (F_i^{\alpha} \times n_i)$ and the reciprocal of the incubation period obtained from the erosion

tests of the various metals at the three standoff distances. Straight lines can be drawn passing through the origin. Therefore, the parameter $\sum(F_i^{\alpha} \times n_i)$ is suitable for the evaluation of cavitation erosion. By using the values of $\alpha$ and C obtained under two different cavitation conditions, we predict the incubation period $t_d$ by Eq. (7) using the values of $F_i$ and $n_i$ obtained at a standoff distance of 4 mm. Fig. 12 shows the relation between the predicted incubation periods and the measured incubation period for the standoff distance of 4 mm, plotted on a double logarithmic scale. A straight line with a slope of 45° on the double logarithmic scale was obtained. This shows that this prediction has a very high accuracy.

In this study, we clarified that the incubation period can be predicted if the constants $\alpha$ and C are obtained by erosion tests and if the bubble collapse impact loads are measured under two different cavitation conditions. Since this result has only been verified at the laboratory level, however, it will be necessary to reseach the applicability of the new erosion prediction method to prototype machine components by measuring the bubble collapse impact loads.
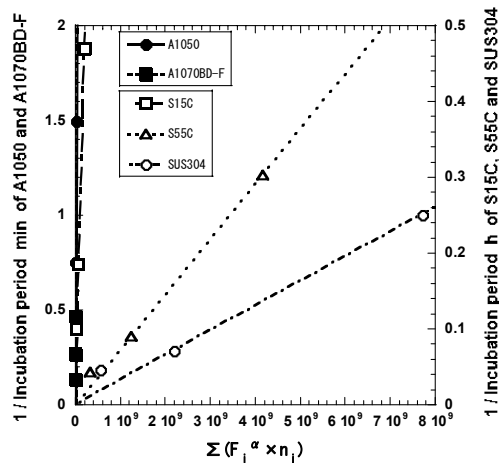


Fig. 11   Relation between $\sum(F_i^{\alpha} \times n_i)$
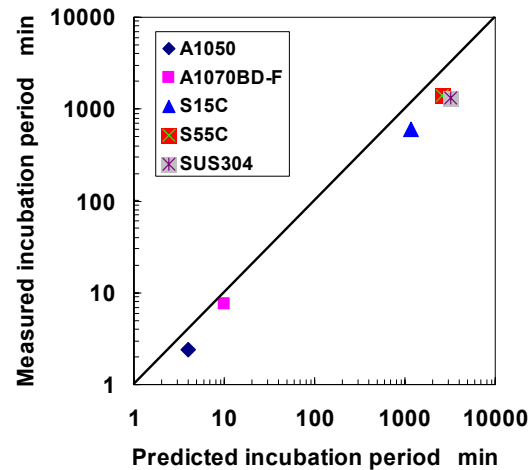and the reciprocal incubation period

Fig. 12   Prediction accuracy
for standoff distance 4 mm

## 4. CONCLUSIONS

In this study, we propose a new prediction method for the incubation period which is based on two sets of erosion tests and on measurements of bubble collapse impact loads. We clarified the following points.

(1) Since the relation between the parameter $\sum(F_i^{\alpha} \times n_i)$ and the reciprocal of the incubation period obtained for various metals shows a proportional relation, the parameter $\sum(F_i^{\alpha} \times n_i)$ is suitable for the evaluation of cavitation erosion.

(2) After the constants $\alpha$ and C of the F-N curve have been obtained under two different cavitation conditions, we can predict the incubation period under yet another condition, provided that the bubble collapse impact loads are measured again.

## REFERENCES

ASTM Designation (2005), G32-03, Annual Book of ASTM Standard, pp. 106-119.

de Jonge, J. B. and Nederveen, A. (1980), ASTM STP 714, pp. 170-184.

De, M. K. and Hammitt, F. G. (1982), Trans. ASTM, Journal of Fluids Engineering, 104, pp. 434-442.

Nakamura, H. (1981), JSMS, Committee on Fatigue of Materials, Research Meeting, No. 158.

Soyama, H. et al. (2007), The 9th AICFM, Jeju, Korea, No. AICFM 9-037.

Hammitt, F. G. (1980) "Cavitation and multiphase flow phenomena", McGraw-Hill Inc., p. 229.

Hattori, S. et al. (1998), Trans. ASME, Journal of Fluids Engineering, Vol. 120, pp. 179-185.

Hattori, S. et al. (1985), Wear, 103, pp. 119-131.

Hattori, S. et al. (2004), Wear, 257, pp. 1022-1029.

Vaidya, S. and Preece, C. M. (1978), Metal Trans. Series A, 9A, 229.

Iwai, Y. et al. (1988), Transactions of the Japan Society of Mechanical Engineers, Series A, Vol. 54, No. 500, pp. 861-867.